JOURNAL OF SPACECRAFT AND ROCKETS
Vol. 31, No. 2, March–April 1994

Three-Dimensional Numerical Investigation of Gravitational and Solutal Effects in a Cylindrical Cell

N. Ramachandran*
Universities Space Research Association, Huntsville, Alabama 35812
and
James Patton Downey†
NASA Marshall Space Flight Center, Huntsville, Alabama 35812

Three-dimensional numerical computations of natural convection in a cylindrical ampoule ($L/R = 4$) are presented for a gallium doped germanium melt. The ampoule is maintained at isothermal end conditions and the g vector is orientated at an angle γ with the horizontal cylinder axis. Detailed velocity, temperature, and concentration field distributions are presented for different gravity levels and for a range of inclination angles ($0 \leq \gamma \leq 180$ deg). For terrestrial conditions ($1g_0$, where g_0 is Earth gravity), complex, multicellular flow is found to occur for $0 \leq \gamma < 180$ deg. The strong convection results in significant isotherm distortions and enhanced heat transfer. As the gravity level is reduced to $10^{-3}g_0$, the overall convection strength decays but the three-dimensional, multicellular flow persists causing appreciable mass transfer. For a further reduction in the gravity level to $10^{-5}g_0$, the system thermal characteristics approach purely diffusive conditions. Flow, thermal, and solutal distributions are presented in the principal, orthogonal, and cross-sectional planes; and the average system heat and mass transfer are calculated.

Nomenclature

A = aspect ratio of cylinder, L/R
C = concentration
e = unit vector
Gr = Grashof number, Ra/Pr
g, g = gravitational acceleration
h = heat transfer coefficient
k = thermal conductivity
L = length of the cylinder
Nu = Nusselt number, Eq. (5)
Pr = Prandtl number, ν/α
p = pressure
R = radius of cylinder, length scale
Ra = Rayleigh number, $g\beta\Delta TR^3/\nu\alpha$
r = radial location
Sh = average Sherwood number, Eq. (6)
T = temperature
t = time
U, V, W = dimensionless velocity components, $(/U_{ref})$
u, v, w = Cartesian velocity components (x,y,z) directions, respectively
U_{ref} = velocity scale, $(\alpha/R)(PrRa)^{1/2}$
X, Y, Z = dimensionless coordinates, $(/R)$
α = thermal diffusivity
β = thermal expansion coefficient
γ = g vector orientation from horizontal cylinder axis
Δ = difference
θ = dimensionless temperature, $2(T - T_r)/\Delta T$
μ = dynamic viscosity
ν = kinematic viscosity
ρ = density
Φ = dimensionless concentration, $2(C - C_r)/\Delta C$
ϕ = azimuthal location

Subscripts
c = cold wall
h = hot wall
r = average value
ref = reference value
x,y = unit vector for direction
0 = terrestrial conditions

Introduction

CRYSTAL growth from melts has received renewed interest in recent years, with the prospect of growing better and larger crystals during extended duration space missions planned for the future. Researchers are constantly striving to improve known techniques and to develop new methods for growing high quality exotic crystals as the technological horizon utilizing these crystals expands on all fronts. Understanding the fundamental transport processes in various crystal growth methods is an important basic step from which shortcomings can be identified and appropriate remedial measures can be contemplated. Most present day crystals are grown with the addition of a solute or dopant to the melt, to yield certain properties desired of the crystal. A homogeneous distribution of the solute in the crystal is critical in obtaining these desired properties. The solute transport is in turn influenced greatly by the convection present in the melt. This study examines the basic convective behavior of a melt and the related heat and solutal transfer in a cylindrical crystal growth cell. Specifically, the effect of the gravity vector g orientation on the convective heat and solutal transfer in a cylindrical cell is investigated.

The study of flow instability in cylindrical cells heated from below has been the subject of many investigations. The onset of axisymmetric and asymmetric convection in such configurations has been examined by linear stability analyses,[1,2] nonlinear analysis,[3] numerical computations,[4–7] and experiments.[8,9] The heated cylinder in a horizontal orientation has also been numerically studied by a number of researchers (see Refs. 9–12 and references cited therein). Experimental and modeling work for this geometry has been done by Schiroky and Rosenberger[13] and Smutek et al.[14] However, the convection phenomenon in inclined cylinders has received considerably less attention. Bontoux et al.[4,15] presented three-dimen-

Presented as Paper 91-1332 at the AIAA 26th Thermophysics Conference, Honolulu, HI, June 24–26, 1991; received Oct. 15, 1991; revision received Feb. 10, 1993; accepted for publication Feb. 10, 1993.

*Associate Scientist. Member AIAA.
†Research Scientist, Space Science Laboratory.

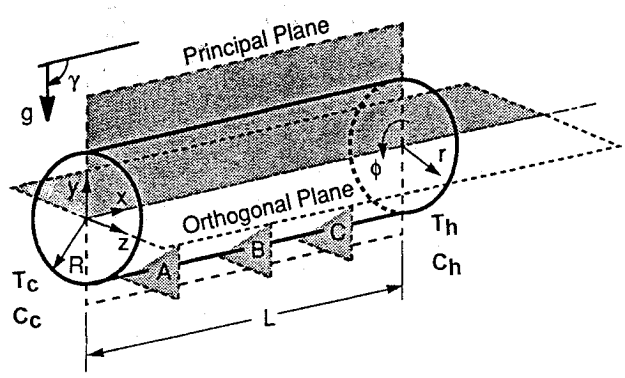

Fig. 1 Schematic of the cylinder geometry; cross-section locations: A, $L/4$; B, $L/2$; C, $3L/4$.

Table 1 System parameters and properties of gallium doped germanium melt

Ampoule radius R, m	0.005
Ampoule length L, m	0.02
ΔT, K	100
μ, kg/m.s	7.28×10^{-4}
ρ, kg/m^3	5.6×10^{3}
ν, m^2/s	1.3×10^{-7}
α, m^2/s	1.3×10^{-5}
β, 1/K	2.50×10^{-4}
D, m^2/s	1.3×10^{-8}
Pr (ν/α)	0.01
Sc (ν/D)	10.0
Gr	1.814×10^{6}

sional numerical solutions for thermal buoyancy driven convection in tilted cylinders and compared their results with data from their experiments. A good qualitative and quantitative agreement between the experiment and the modeling effort was reported. The study considered a slender cylinder ($A = L/R = 10$) with $Ra = 20{,}000$ and inclination angles up to 60 deg from the horizontal. Velocity and isotherm distributions were reported; but the system heat transfer was not characterized. Recently, results from numerical experiments on the Bridgman directional solidification of GaAs were reported by Arnold et al.[16] Their results showed that when the g vector (magnitude $10^{-5}g_0$) was perfectly aligned to the ampoule axis (bottom heated case), the flow was axisymmetric (four cell behavior). When the resultant g vector was tilted by as little as 0.05 deg from the axis, the flow displayed a transitional behavior to asymmetric convection, which completely dominated the cell at $\gamma = 0.5$ deg. Very limited studies on combined solutal and thermal transfer have been reported in surveyed literature. Results from a numerical study of Soret separation of a two component binary mixture in microgravity were reported by Henry and Roux.[17]

The past experimental and numerical investigations have all revealed complex flow behavior in cylindrical cells that is dependent on a number of factors. For instance, the cylinder orientation, heating conditions, aspect ratio, the Rayleigh and Prandtl numbers of the fluid, all play a significant role in influencing the flow characteristics. In most instances, the flow is asymmetric and degenerates into oscillatory motion when Ra is increased. Even experiments in space have been found to be affected by convective instabilities.[17] The study of convection within cylinders that are inclined at an arbitrary angle with respect to the gravity vector are of particular interest to researchers in the microgravity program, since small, steady accelerations do occur in orbit and it is difficult to align the direction of these accelerations with the axis of the crystal growth cell. The effect of the g vector orientation and magnitude on such crystal growth and fluids experiments has yet to be fully understood. This study aims to gain a better understanding of the fluid mechanics, and heat and mass transfer associated with some of these flows.

Geometry Description and Solution Strategy

A schematic of the cylinder geometry used in the investigation is shown in Fig. 1. It consists of a right circular cylindrical cell ($A = L/R = 4$) with differentially heated end walls. As shown in the figure, the g vector is orientated at an angle γ from the horizontal cylinder axis. The end walls are maintained at isothermal temperatures T_h and T_c with $T_h > T_c$. Thus, for this geometry, $\gamma = 0$ deg corresponds to the bottom heated case. A linear temperature profile is prescribed for the cylinder side wall which corresponds to a purely diffusive wall behavior (conduction). The end wall boundary conditions for solute transport are similar to the temperature conditions with $C = C_c$ at $x = 0$ and $C = C_h$ at $x = L$, with $C_h > C_c$. However, a zero solutal gradient condition is imposed on the azimuthal cylinder wall. This boundary condition (Neumann-type gradient condition) is more appropriate than a prescribed value (Dirichlet-type condition) because the solute is present in

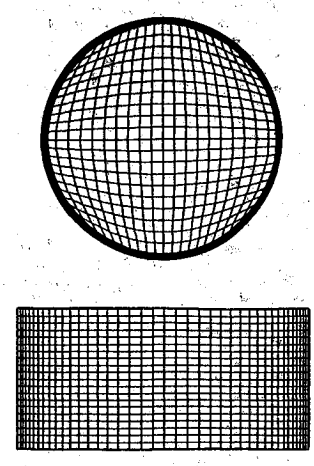

Fig. 2 Boundary fitted coordinate grid, 41 × 21 × 21.

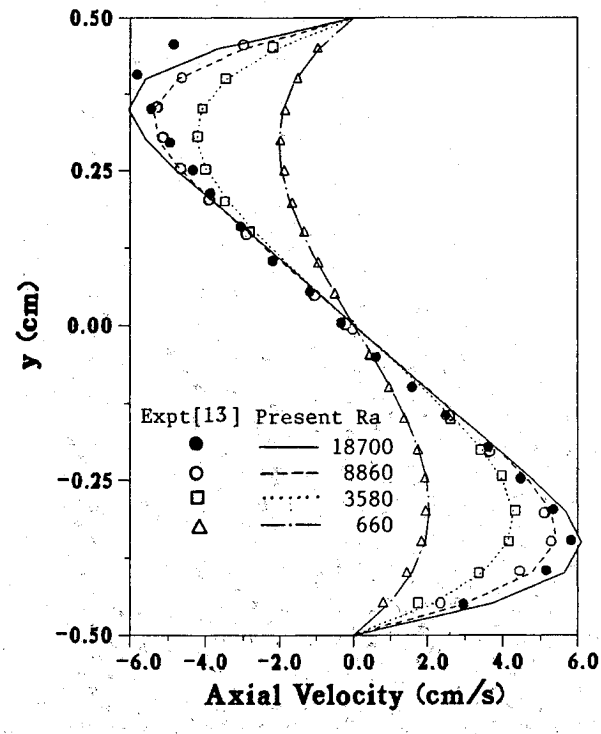

Fig. 3 Comparisons between computations and experimental results for a heated horizontal cylinder.

the melt only in small quantities as a dopant and has a relatively small diffusion coefficient compared to the high conductivity of the melt. The convective motion is driven by the thermal buoyancy force generated in the melt due to the imposed axial temperature gradient. Contributions due to solutal buoyancy are assumed to be negligible and, hence, are not included in this study. The principal (x-y), orthogonal (x-z) cylinder planes, as well as the axial locations of cross-sectional planes (A, B, and C) are identified in the figure. These planes will be used in later sections to present vector and scalar distributions. The differential equations governing the transport of mass, momentum, energy, and species in the system are the conservation equations for mass (continuity), momentum (three-dimensional incompressible Navier-Stokes equations for a Boussinesq fluid), temperature, and concentration. No-slip velocity conditions are imposed on the cylinder walls and the temperature/concentration conditions are as mentioned previously. A gallium doped germanium melt is modeled in the present investigation and the relevant system and melt properties are summarized in Table 1. The governing equations are cast into nondimensional form using scale factors for length R, velocity U_{ref}, temperature $\theta = 2(T - T_r)/(T_h - T_c)$ and concentration $\Phi = 2(C - C_r)/(C_h - C_c)$. The transformed equations are shown next in vector form.

$$\nabla \cdot v = 0 \tag{1}$$

$$v_t = -\nabla p - (v\nabla)v + (Gr - \tfrac{1}{2})\nabla^2 v - e_x \cos\gamma(\theta/2) + e_y \sin\gamma(\theta/2) \tag{2}$$

$$\theta_t = -v \cdot \nabla\theta + (Pr\,Ra) - \tfrac{1}{2}\nabla^2\theta \tag{3}$$

$$\Phi_t = -v \cdot \nabla\Phi + (Sc^{-1}\,Gr - \tfrac{1}{2})\nabla^2\Phi \tag{4}$$

The equations and boundary conditions are solved by a three-dimensational solver set up in generalized body-fitted (curvilinear) coordinates.[18] The transport equations are discretized by finite difference approximations using an upwind scheme based on second-order central differences with artificial damping for the convective terms and standard central differences for the remaining terms. A pressure-based predictor, multicorrector solution procedure[19] is employed to ensure velocity-pressure coupling and divergence-free flowfield solutions. To validate the code, numerical simulations were carried out for the horizontal cylinder problem ($\gamma = 90$ deg).

This problem has been experimentally investigated by Schiroky and Rosenberger[13] using pressurized gases for a range of Rayleigh numbers and for a cylinder with an aspect ratio $L/R = 10$. Detailed velocity distributions were measured using laser Doppler velocimetry at various axial locations in the cylinder. Cases 2, 4, 6, and 7 in their investigation[13] were chosen for simulation in the validation exercise. A $41 \times 21 \times 21$ grid (x, y, and z directions, respectively) was used in the computations, and the grid distribution is shown in Fig. 2. Computations were carried out until a convergence criteria, $\epsilon = 10^{-5}$, was attained for the sum of the normalized residuals for the momentum, pressure correction, energy, and concentration equations. Convergence was typically attained in about 300 time steps, corresponding to a CPU time of about 8 min on a Cray XMP computer. Comparisons between the measured and computed velocity profiles in the principal plane and at axial location $x = L/2$ are presented in Fig. 3. Very good agreement between the two results is evident at all but the highest Rayleigh number investigated. Present computations for $Ra = 18{,}700$ predict the peak velocity magnitude correctly, but the location of this peak is shifted with respect to the measurements. It is to be noted that the measurements[13] for this value of Ra, are not symmetric across the centerline ($y = 0$), with a slight outward shift observed in the upper-half of the plane. No runs were repeated with further grid refinement, and the level of agreement seen in the figure between the computations and measurements was deemed adequate for code validation purposes. It may be added that the code has also been successfully tested against transient two- and three-dimensional benchmarks for different Reynolds number flows.[19]

Results and Discussion

Numerical simulations for the gallium doped germanium melt were carried out for the following terrestrial and reduced gravity situations:

1) Gravity $g = 1g_0$ and $\gamma = 0$, 45, 90, 135, and 180 deg.
2) Gravity $g = 10^{-3}g_0$ and $\gamma = 0$, 10, 20, 30, 45, 90, 135, and 180 deg.
3) Gravity $g = 10^{-5}g_0$ and $\gamma = 0$, 45, 90, 135, and 180 deg.

All of the calculations were performed for cell dimensions noted in Table 1 and for a temperature difference $\Delta T = 100$ K. Since the gravity effect on the melt is reflected as the thermal buoyancy force Ra in the governing equations, results for case 2 noted earlier can also be interpreted as the results for $g = 10^{-5}g_0$ and $\Delta T = 10^4$ K (a two-order increase in the temperature difference over case 3). In all of the simulations, the same grid distribution adopted previously ($41 \times 21 \times 21$, Fig. 2) was employed. The computation time for each run, however, was significantly increased due to the slow convergence

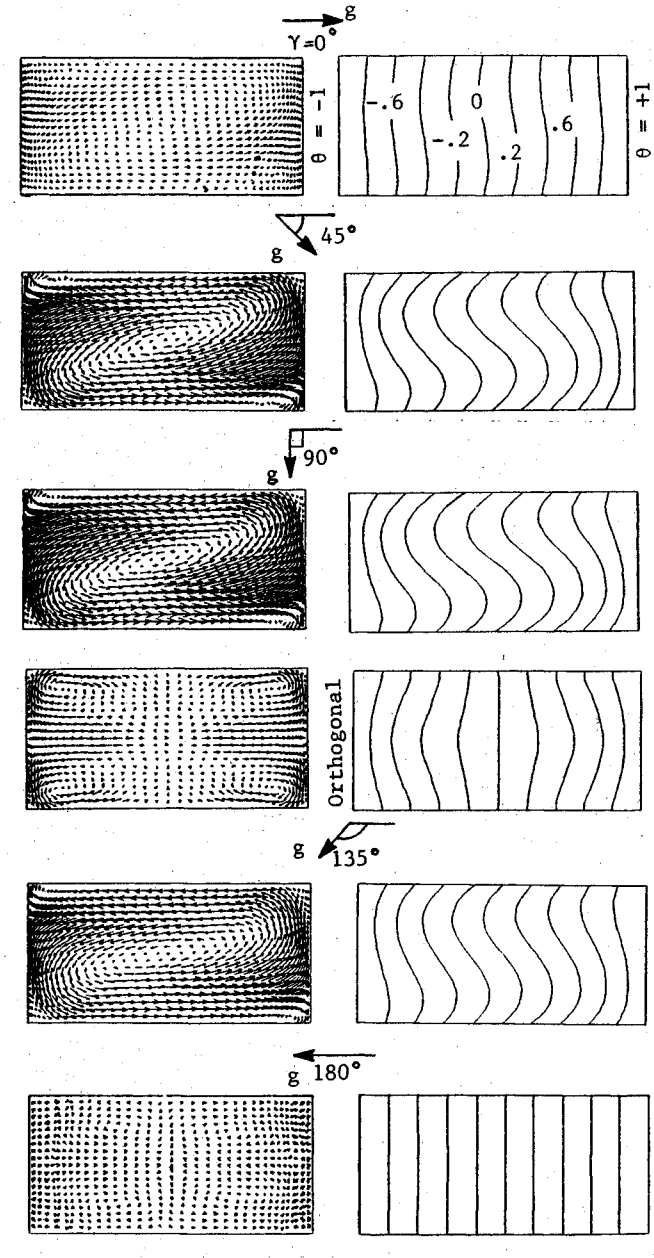

Fig. 4 Velocity vector and isotherm distributions; $g = 1g_0$.

of the concentration equation. This is due to the lower diffusivity of gallium ($Sc = 10$) compared to the thermal conductivity of germanium ($Pr = 0.01$). Typically, 800–1500 time steps were required to achieve convergence ($\epsilon = 10^{-5}$). In the following sections, detailed velocity, isotherm and isomer (constant concentration) distributions will be presented for representative cases. The average heat and mass transfer will also be presented as dimensionless Nusselt and Sherwood numbers defined as

$$Nu = {}_{\text{area}} \int (\mathrm{d}\theta/\mathrm{d}X)\, \mathrm{d}Y\, \mathrm{d}Z \tag{5}$$

$$Sh = {}_{\text{area}} \int (\mathrm{d}\Phi/\mathrm{d}X)\, \mathrm{d}Y\, \mathrm{d}Z \tag{6}$$

Terrestrial Gravity ($g = 1g_0$, $Ra = 1.814 \times 10^4$)

Steady-state results were obtained for five inclination angles (ranging from $\gamma =$ 0–180 deg) for a system Rayleigh number $Ra = 1.814 \times 10^4$. A sampling of the velocity vector and isotherm distributions is presented in Fig. 4. The distributions are for the principal plane identified in Fig. 1, except for $\gamma =$ 90 deg, for which the flow and thermal fields are also presented for the orthogonal (x-z) plane. Identical velocity scaling is adopted for all vector plots to facilitate magnitude comparisons. The g vector orientation with respect to the cylinder axis is also shown for each case.

Flow Characteristics and Heat Transfer

For all of the situations where convection exists (all of the cases except $\gamma = 180$ deg), the flowfield exhibits multicellular behavior, with the thermal field showing appreciable effects of the convective flow. For $\gamma = 0$ deg (bottom heated case), one major counter-clockwise (CCW) circulation cell is clearly visible along with counter-rotating-clockwise (CW) vortices located at the cell corners. Such asymmetric convective behavior is predicted by linear theories[1,2] and was also numerically computed by Crespo et al.[5] for Prandtl numbers (0.02, 0.7, and 6.7). The incipience of asymmetric convection has been shown[1,2] to occur in bottom heated cylinders with an aspect ratio $A \simeq 1.6$. At lower values of the Rayleigh number, only one asymmetric cell is found to occupy the entire cell, with the longitudinal flow being essentially parallel to the axis. As the Rayleigh number is increased, the primary convection pattern is found to incline to the cylinder axis, and the beginnings of the corner vortices are observed.[5] The overall convection strength is seen to increase as γ is increased to 90 deg, after which the circulation strength starts to decay. For $\gamma = 180$ deg (stably stratified orientation), there is no flow present in the cell as no driving buoyancy force exists for this orientation. It is also noted that for all of the cases where convection is present, the main flow cell is found to be inclined to the cylinder axis, similar to the findings in Ref. 5 for a vertical cylinder. The development of boundary layers is also evident in all of these cases. Attention to the flow pattern in the orthogonal plane for $\gamma = 90$ deg shows the presence of four recirculating cells. Similar behavior was reported in Ref. 4 where convection inside a vertical cylinder ($A = 2$) was numerically investigated. In the present investigation, this four cell behavior is found to be feeble for $\gamma = 0$ deg and strongest for the horizontal case ($\gamma = 90$ deg, shown in Fig. 4). Isotherms in this instance, shown alongside the vector plot, show them drawn away by the convective flow from the center to the end walls. As γ is increased further, the four cell behavior is found to persist but the convective flow strength is attenuated.

The isotherm distributions in the principal plane shown in Fig. 4 echo the flow characteristics discussed in the previous section. They are drawn by the flow from the hot to the cold wall in the upper-half of the cylinder and show the opposite trend in the lower-half of the cylinder. It is to be noted that the melt has a high thermal conductivity and, hence, no severe temperature gradients are observed in the system for any case. On the other hand, solute computations for this case showed very strong concentration gradients which were not resolved

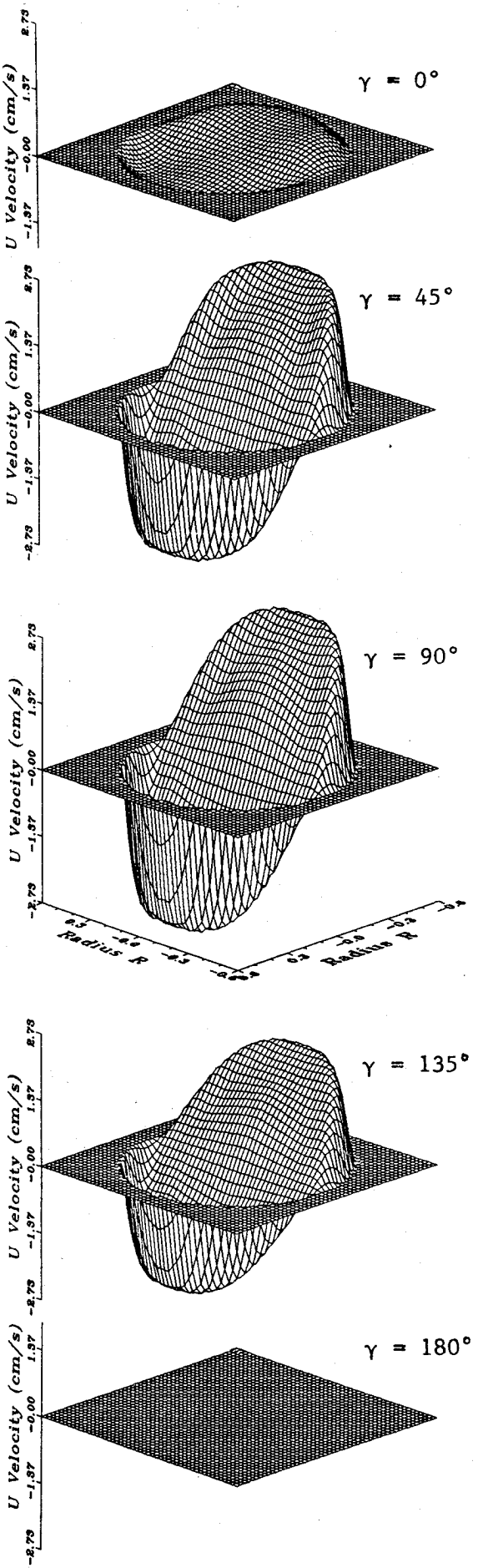

Fig. 5 Axial velocity variation with inclination angle; $g = 1g_0$.

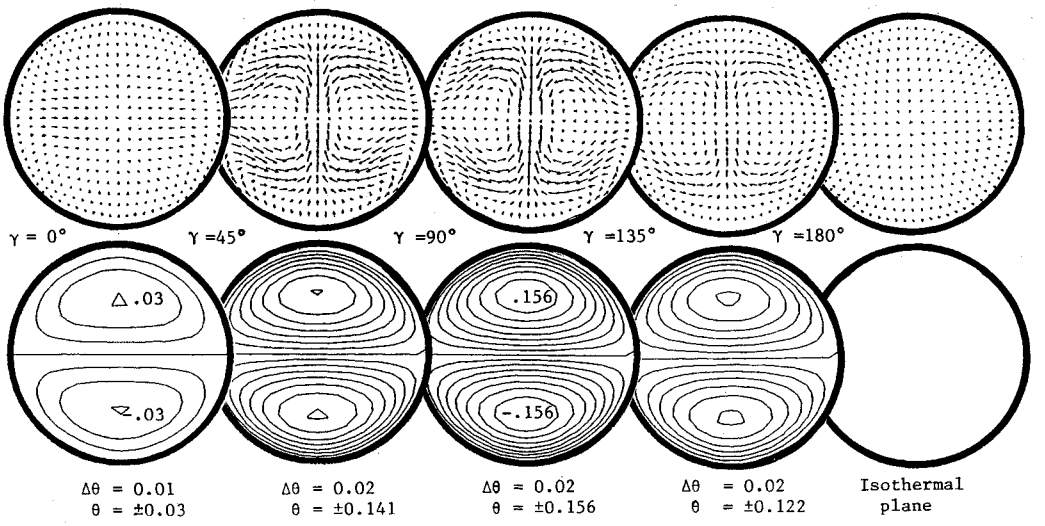

Fig. 6 Cross-sectional velocity and isotherms; section B, $g = 1g_0$.

by the relatively coarse grid used in the investigation. Detailed computations with a finer grid to correct this problem are part of a separate investigation. The overall system heat transfer that is characterized by the average Nusselt number will be discussed in a later section. The axial velocity u distributions at $x = L/2$ is shown in Fig. 5 as surface plots for different inclination angles. For $\gamma = 0$ deg, the core velocity resembles an S curve. As γ is increased to 45 deg, the velocity maximum is shifted toward the cylinder wall, and the flow shows a characteristic boundary-layer type Z profile. The flow displays a more or less linear distribution across the cylinder cross section, between the flow maximum and minimum values. Some departures from this linear behavior are seen at the outer edges of the core surface. At $\gamma = 45$ deg, the flow (u velocity) is already close (8.2%) to the maximum value which is attained at $\gamma \simeq 90$ deg. Previous research[14] has shown that in long horizontal cylinders with $Ra \leq 3580$ the axial velocity component in the core can be predicted quite accurately by asymptotic theory. For $Ra \geq 3580$, however, the flow exhibits a boundary-layer type behavior, and the analytical predictions show marked deviations from measured velocity profiles. In the present study, velocity profiles for $\gamma = 45$, 90, and 135 deg all show boundary-layer type behavior. For a further increase in the tilt angle ($\gamma = 135$ deg), flow decay is clearly evident with the maximum value now being 75.4% of that at $\gamma = 90$ deg. The location of this maximum is also seen to shift away from the cylinder wall. At $\gamma = 180$ deg, no discernible flow is present as the fluid is stably stratified. It may be pointed out that the maximum u velocity (located at $x \simeq L/2$) is found to be within 5% of the maximum system velocity. The contributions due to v and w components are thus minimal for all of the angles. For example, the maximum system velocities for $\gamma = 0$ deg and $\gamma = 90$ deg are 0.483 cm/s and 2.733 cm/s, respectively, and the corresponding maximum u velocities are 0.468 cm/s and 2.732 cm/s, respectively. Cross-sectional velocity and isotherm plots at section B ($x = L/2$) are shown in Fig. 6 for the different tilt angles investigated. A multicellular behavior is noticed at $\gamma = 0$ deg. As γ is increased, this flow waxes and wanes in strength with the horizontal station ($\gamma = 90$ deg) representing the maximum flow location. The isotherms also show the increase and decrease in heat transfer with the inclination angle. This effect is quantified by the isotherm contour values included in the figure. It is interesting to note that the isotherms show symmetry about the centerline even though the main flow (principal plane) is inclined to the cylinder axis. This is because for the present setup ($A = 4$), only a single dominant circulation cell is present, and the flow is essentially parallel to the cylinder axis in the vicinity of section B. It will be seen later that concentration profiles at sections A and C that are far removed from the half-length location do not display the aforementioned symmetry.

Reduced Gravity ($g = 10^{-3}g_0$, $Ra = 18.14$)

Detailed computations for this case are carried out for $\gamma = 0$, 10, 20, 30, 45, 90, 135, and 180 deg. For $\gamma = 0$ deg, the Rayleigh number is below the critical value required to trigger convection. For $A = 4$, the critical Rayleigh number has been calculated to range from 1041 (see Ref. 2) to 1114 (Ref. 1). Thus, both $\gamma = 0$ deg and $\gamma = 180$ deg represent no-flow situations and the melt is found to be linearly stratified with respect to the temperature and concentration fields. As the cylinder axis is tilted slightly ($\gamma = 10$ deg) with respect to the g vector orientation, a circulation cell driven by thermal buoyancy is observed. This cell is found to occupy the entire cylinder (in the principal plane) and no secondary corner vortices are perceived. This single cellular behavior is noticed at all the inclination angles for which convection is present. Although moderate convection is seen for 30 deg $\leq \gamma \leq$ 135 deg, the isotherms are not affected by the flowfield due to the low melt Prandtl number. This points to the fact that in a reduced gravity environment, flat crystal interfaces can be successfully obtained. Thus, the average Nusselt number is equal to 1.0 (pure diffusive behavior) for all of the simulations. The solute field, however, shows significant convection effects as discussed in the next section.

Flow Characteristics, Heat and Mass Transfer

Results for $\gamma = 90$ deg are typical of the overall results calculated for this situation. Principal, orthogonal, and cross-sectional plane plots for this geometry are presented in Figs. 7 and 8, respectively. The flow, thermal, and solutal fields are shown in Fig. 7, whereas only the flow and solutal field distributions are shown in Fig. 8 since the cross-sectional planes are isothermal. Inferences drawn from these figures are now presented sequentially, starting first with Fig. 7.

1) A single flow cell is seen in the principal plane with a maximum u velocity of 0.0145 cm/s. This compares to a maximum axial velocity of 2.733 cm/s for $1g_0$ and the same angle of inclination. In the orthogonal plane, however, the four cell (symmetric) behavior seen for $1g_0$ is recaptured; the flow velocities in the vortices, however, are considerably reduced in magnitude.

2) Both the principal and orthogonal plane isotherm distributions show a purely diffusive behavior. No flowfield effects are reflected on the system heat transfer. This behavior persists at all inclination angles.

3) However, the solute field shows a strong influence of convection in the melt. The isomers are drawn in the direction

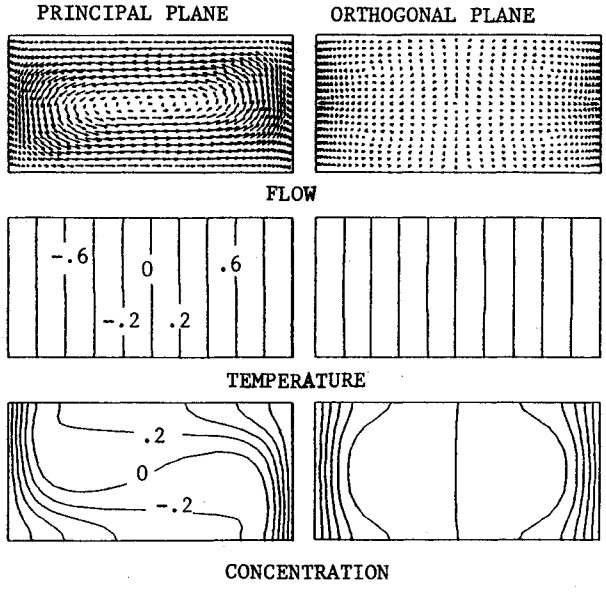

Fig. 7 Velocity, temperature, and concentration fields; $\gamma = 90$ deg and $g = 10^{-3}g_0$.

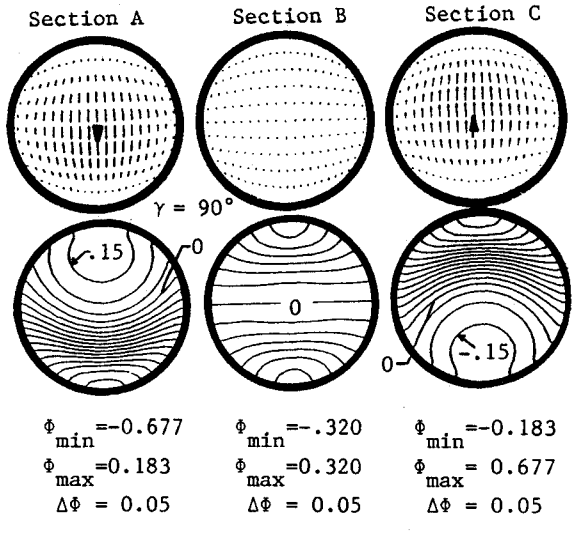

Fig. 8 Flow and concentration profiles at cross section B; $\gamma = 90$ deg and $g = 10^{-3}g_0$.

of the flow in both the principal and orthogonal planes and show appreciable distortions. Since Ra is significantly lower than the $1g_0$ case, the $41 \times 21 \times 21$ grid is adequate to resolve the solute boundary layers in the melt. The isomer distributions are found to be symmetric about the vertical centerline in the orthogonal plane.

4) Strong solutal gradients are observed near the cylinder end walls that translate into considerable mass transfer in these regions. The average Sherwood number variation with γ will be discussed in a subsequent section.

5) The isomers in the principal and orthogonal planes also suggest the existence of a core volume in the melt (with boundaries approximately $0.5R$ from all solid walls), where the solute field is essentially uniform. This represents a layer characterized by low velocities.

The following inferences are based on cross-sectional plots shown in Fig. 8.

6) The flowfield essentially shows fluid rising near the hot end of the cylinder (section C) and descending adjacent to the cold end (section A). At the midsection B, fluid convection is very feeble and a dominant flow pattern is not evident.

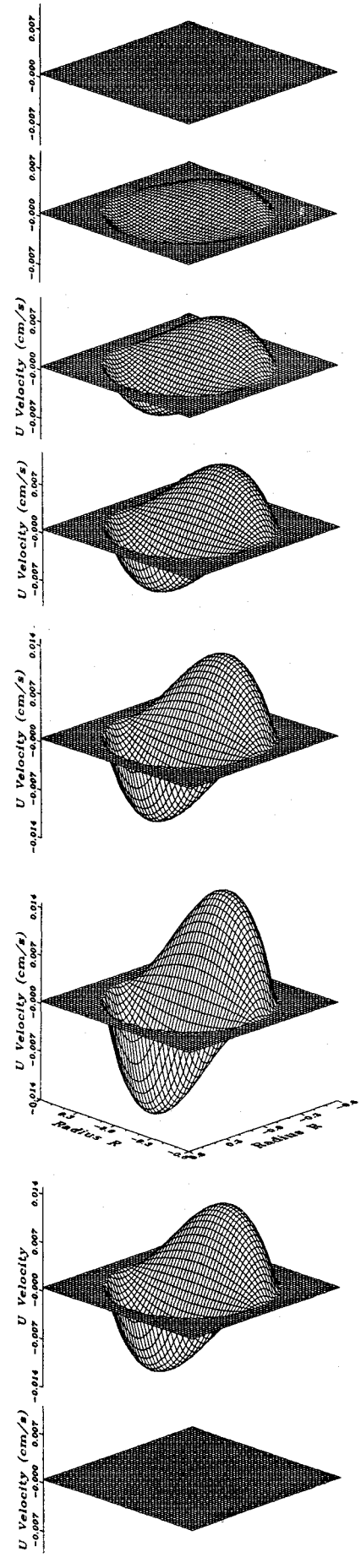

Fig. 9 Surface plots of axial velocity, section B; $g = 10^{-3}g_0$. From top $\gamma = 0$, 10, 20, 30, 45, 90, 135, and 180 deg.

7) Since the thermal field is linearly stratified (axial direction), the isotherms show no variation across the cross-sectional planes and, hence, are not included in the figure.

8) However, the solute field shows significant response to the convective flow and reflects the flow behavior. Section *C* shows the upward migration of isomers due to the upward buoyant flow, and section *A* contours show the downward shift of isomers due to the downwelling flow. The symmetry observed at section *B* about the horizontal centerline indicates the presence of localized symmetric flows in this region.

It may be mentioned here, that for the other angles investigated, similar trends are noticed in the flow, temperature, and solute fields although to varying degrees. Maximum convective strength is observed at $\gamma = 90$ deg, and the solute fields also show maximum isomer distortions for this inclination angle.

Surface plots of the axial velocity are presented in Fig. 9 for all of the cases that were computed. The gradual buildup of the buoyancy force as a function of increasing inclination angle is clearly evident. A maximum value is attained at $\gamma = 90$ deg, and the flow decays subsequently to still conditions (no convection) at $\gamma = 180$ deg. For all of the angles where convection is present, the flow profiles are S shaped in contrast to the Z profiles seen for $1g_0$.

Microgravity ($g = 10^{-5}g_0$)

Computer simulations for the microgravity environment show diffusion dominated thermal and solutal transports. Even though feeble convection is observed, the isomer distortions are minimal. A sampling of principal-plane flow and solute distributions and isomers in a cross-sectional plot (section *B*) are presented in Fig. 10 for $\gamma = 90$ deg (maximum convection strength). A single circulation cell seen in the longitudinal plane causes the concentration distribution seen in section *B*. The isomer response to the flow is very subdued in contrast to that seen for $10^{-3}g_0$. Incidentally, results for $10^{-3}g_0$ can be interpreted as results for $10^{-5}g_0$ (microgravity) but with a system $\Delta T = 10^4$ K. As the imposed temperature gradient is increased, the convection strength is augmented which, in turn, increases the system heat and mass transfer. The maximum system velocity is $\simeq 1.5$ μm/s for $\gamma = 90$ deg. It is even lower at the other inclination angles. It may be noted here that at this gravity level, the velocities are of the same order as typical translation rates of crystal growth cells in a furnace; approximately 1 mm/h ($\simeq 0.3$ μm/s). This is of particular importance in obtaining crystals of good quality. Brown[20] and references cited therein predicted that radial segregation of solute in a crystal reaches a maximum at acceleration levels that induce convective flows of the same magnitude as the crystal interface translation rate. The reason for this prediction is as follows. At high convective flows, segregation is minimized due to strong mixing. As the flow decreases, mixing becomes poor and segregation increases. The maximum segregation occurs when flows are just strong enough to transport material from the advancing interface but are not strong enough to recirculate the material throughout the melt. For still weaker flows, there is insufficient flow to cause significant segregation to develop at the crystal interface, and a crystal with good radial uniformity is obtained. Examination of results from the present computations shows that a crystal grown at $Ra = 0.1814$ ($10^{-5}g_0$) will exhibit a larger degree of radial segregation than the one grown at $Ra = 18.14$ ($10^{-3}g_0$). Thus microgravity may actually prove deleterious in this particular instance.

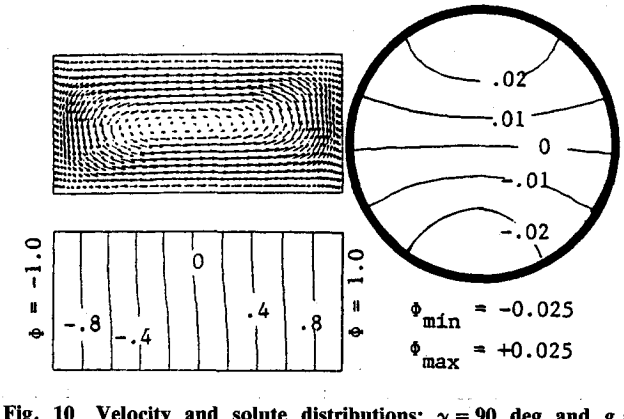

Fig. 10 Velocity and solute distributions; $\gamma = 90$ deg and $g = 10^{-5}g_0$.

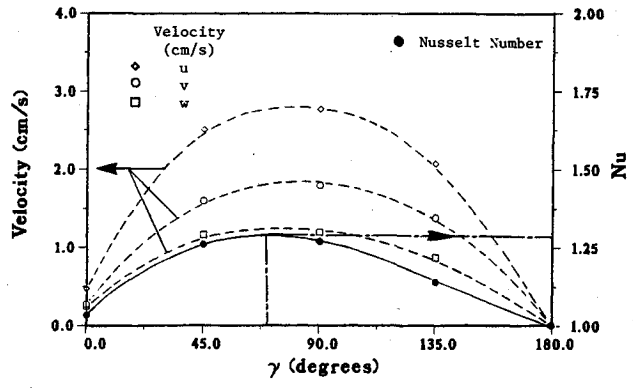

Fig. 11 Variation of average Nusselt number and maximum velocities with inclination angle, $g = 1g_0$.

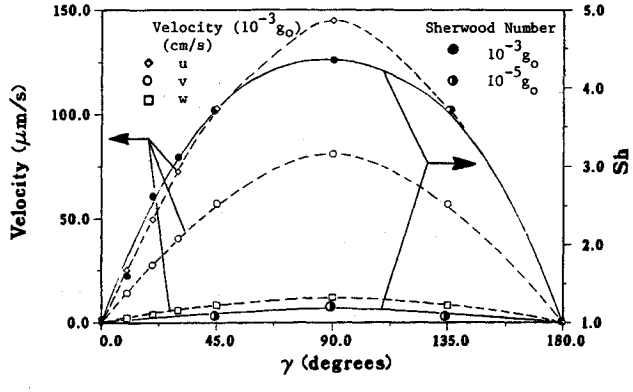

Fig. 12 Variation of mass transfer and maximum velocities with inclination angle, $10^{-3}g_0$ and $10^{-5}g_0$.

System Heat and Mass Transfer

The overall system heat transfer is presented in Fig. 11 for terrestrial gravity conditions, $1g_0$. Also shown in the figure, are the maximum u, v, and w velocities for various inclination angles. For $\gamma = 0$ deg, the average Nusselt number is 1.03 (>1.0, pure diffusion) due to the presence of convection (u, v, $w > 0.0$). As the inclination angle is increased, convection becomes more vigorous and results in enhanced heat transfer. The Nusselt number attains a maximum value of $\simeq 1.30$ at $\gamma \simeq 70$ deg, before dropping down to 1.0 at $\gamma = 180$ deg. This correlates to the velocity behavior that also shows a maximum at $\gamma \simeq 70$ deg. Two-dimensional computations of natural convection in side-heated rectangular, tilted enclosures[21] also showed a similar heat transfer behavior, yielding a maximum Nu at $\gamma = 60$ deg. The computations were for $Pr = 10$ and $Ra = 2000$–8000. As mentioned earlier, the u velocity is the dominant velocity in the system followed by v and w components in that order. The maximum u occurs at $x \simeq L/2$, and the maximum v and w are both located at $x \simeq 0.97L$ (adjacent to the hot end wall).

Average Sherwood numbers for $g = 10^{-3}g_0$ and $10^{-5}g_0$ are plotted in Fig. 12 as a function of the inclination angle. Also included in the figure are the maximum velocities for the

$10^{-3}g_0$ case. The average Nusselt number is equal to 1.0 for both these gravity values and does not show any effect of the inclination angle. The *Sh* curve for $10^{-3}g_0$ does not show the skewness observed in the heat transfer behavior for $1g_0$, and the occurrence of the maximum also coincides with the velocity maximum. It appears that the incipience of the corner vortices contribute to the skewed heat transfer behavior at $1g_0$. The maximum calculated u velocity ($\simeq 150$ μm/s) is two orders of magnitude lower than the u_{max} at $1g_0$ ($\simeq$ 2.7 cm/s). Velocities for $10^{-5}g_0$ are < 2 μm/s and similarly represent a two order of magnitude reduction from the $10^{-3}g_0$ case.

Conclusions

Three-dimensional computations of natural convection in a tilted cylindrical cell are reported for terrestrial and reduced gravity environments. The calculations were carried out for a gallium doped germanium melt with the cylinder end walls maintained under isothermal conditions and the azimuthal wall assumed to be perfectly conducting. Results from the computations show that for the $1g_0$ case, the flow is multicellular both in the principal and orthogonal planes and causes appreciable heat transfer in the system. The flow and temperature fields show boundary-layer characteristics, and the maximum flow velocity and heat transfer is computed for $\gamma \simeq 70$ deg. The inadequate resolution of the solutal boundary layer by the coarse grid used in the computations precluded the calculation of the solutal distributions for $1g_0$. For $g = 10^{-3}g_0$ (reduced gravity), the melt is linearly stratified with respect to the thermal field, but the solute field shows significant effects of the convective flow. There is no convection at $\gamma = 0$ deg since the system *Ra* is below the critical value. The four cellular behavior seen for $1g_0$ is recaptured in the orthogonal plane, but in the principal plane a single recirculation cell occupies the entire calculation domain. The maximum system velocity ($\simeq 150$ μm/s) occurs at $\gamma = 90$ deg, and the maximum mass transfer is also calculated at this tilt angle. The axial velocity distributions display S profiles in contrast to the Z-type profiles perceived at $1g_0$. For a further reduction in the gravity level to $10^{-5}g_0$, some isomer distortions are evident due to a feeble convection in the melt (maximum velocity < 2 μm/s). The thermal field is linearly stratified as before, and the solute field approaches diffusive behavior. The results show that for a crystal growth problem, reduced gravity can assist in obtaining good quality crystals by providing flat growth interfaces due to isothermal cross sections. However, radial segregation could be more pronounced at $10^{-5}g_0$ than at higher g levels and this could be a potential problem. This problem may be alleviated by the choice of different system physical parameters to further reduce the Rayleigh number. The calculations further show that under microgravity conditions (for cases where convection is present), the inclination angle γ has minimal effect on the flow and mass transfer of the system.

References

[1]Charlson, G. S., and Sani, R. L., "On Thermoconvective Instability in a Bounded Cylindrical Fluid Layer," *International Journal of Heat and Mass Transfer*, Vol. 14, No. 12, 1971, pp. 2157–2160.

[2]Buell, J. C., and Catton, I., "The Effect of Wall Conduction on the Stability of a Fluid in a Right Circular Cylinder Heated form Below," *Journal of Heat Transfer*, Vol. 105, No. 2, 1983, pp. 255–260.

[3]Rosenblat, S., "Thermal Convection in a Vertical Circular Cylinder," *Journal of Fluid Mechanics*, Vol. 122, Sept. 1982, pp. 395–410.

[4]Bontoux, P., Smutek, C., Randriamampianina, A., Roux, B., Extremet, G. P., Schiroky, G. H., Hurford, A. C., and Rosenberger, F., "Finite Difference Solutions for Three-dimensional Buoyancy Driven Flows in Inclined Cylinder," *Numerical Methods for Non-linear Problems*, edited by C. Taylor, D. R. J. Owen, E. Hinton, and F. B. Damjanic, Pineridge Press, Swansea, England, UK, 1986, pp. 1102–1115.

[5]Crespo, E., Bontoux, P., Smutek, C., Roux, B., Hardin, G., Sani, R., and Rosenberger, F., "Three dimensional Simulations of Convection Regimes in Cylindrical Ampoules—Comparisons with Theoretical Analyses and Experiments," *Proceedings of the 6th European Symposium on Material Sciences under Microgravity Conditions*, (Bourdeaux, France), ESA Publications Div., The Netherlands, Dec. 1986, pp. 529–537.

[6]Kirchartz, K. R., Mueller, U., Oertel, H., Jr., and Zierep, J., "Axisymmetric and Nonaxisymmetric Convection in a Cylindrical Container," *Acta Mechanica*, Vol. 40, No. 4, 1981, pp. 181–194.

[7]Behinger, R. P., and Ahlers, G., "Heat Transfer and Temporal Evolution of Fluid Flow near the Rayleigh Bernard Instability in Cylindrical Containers," *Journal of Fluid Mechanics*, Vol. 125, Dec. 1982, pp. 219–258.

[8]Mueller, G., Neumann, G., and Weber, W., "Natural Convection in Vertical Bridgman Configurations," *Journal of Crystal Growth*, Vol. 70, Nos. 1/2, 1984, pp. 78–93.

[9]Olson, J. M., and Rosenberger, F., "Convective Instabilities in a Closed Vertical Cylinder Heated from Below, Part 1, Monocomponent Gases," *Journal of Fluid Mechanics*, Vol. 92, June 1979, pp. 609–629.

[10]Martini, W. R., and Churchill, S. W., "Natural Convection inside a Horizontal Cylinder," *AIChE Journal*, Vol. 6, No. 2, 1960, pp. 251–257.

[11]Leong, S. S., and De Vahl Davis, G., "Natural Convection in a Horizontal Cylinder," *Numerical Methods in Thermal Problems*, edited by W. Lewis and K. Morgan, Pineridge Press, Swansea, England, UK, 1979, pp. 287–296.

[12]Bejan, A., and Tien, C. L., "Fully Developed Natural Convection Counterflow in a Long Horizontal Pipe with Different End Temperatures," *International Journal of Heat and Mass Transfer*, Vol. 21, No. 6, 1978, pp. 701–708.

[13]Schiroky, G. H., and Rosenberger, F., "Free Convection of Gases in a Horizontal Cylinder with Differentially Heated End Walls," *International Journal of Heat and Mass Transfer*, Vol. 27, No. 4, 1984, pp. 587–598.

[14]Smutek, C., Bontoux, P., Roux, B., Schiroky, G. H., Huford, A. C., Rosenberger, F., and De Vahl Davis, G., "Three Dimensional Convection in Horizontal Cylinders: Numerical Solutions and Comparison with Experimental and Analytical Results," *Numerical Heat Transfer*, Vol. 8, No. 5, 1985, pp. 613–631.

[15]Bontoux, P., Smutek, C., Randriamampianina, A., Roux, B., Extremet, G. P., Hurford, A. C., Rosenberger, F., and De Vahl Davis, G., "Numerical Solutions and Experimental Results for Three Dimensional Buoyancy Driven Flows in Tilted Cylinders," *Advances in Space Research*, Vol. 6, No. 5, 1986, pp. 155–160.

[16]Arnold, W., Jacqmin, D., Gaug, R., and Chait, A., "Convection Phenomena in Low-Gravity Processing: the GTE GaAs Experiment," AIAA Paper 90-0409, Jan. 1990.

[17]Henry, D., and Roux, B., "Numerical Simulation of 3D Convective Motion disturbing the Soret Separation of the two Components of a Binary Mixture," *Advances in Space Research*, Vol. 6, No. 5, 1986, pp. 141–146.

[18]Chen, Y. S., "A Computer Code for Three Dimensional Incompressible Flows Using Nonorthogonal Body Fitted Coordinate Systems," NASA CR-178818, March 1986.

[19]Chen, Y. S., "Compressible and Incompressible Flow Computations with a Pressure Based Method," AIAA Paper 89-0286, Jan. 1989.

[20]Brown, R. A., "Theory of Transport Processes in Single Crystal Growth from Melt," *AIChE Journal*, Vol. 34, No. 6, 1988, pp. 881–911.

[21]Ozoe, H., Yamamoto, K., Sayama, H., and Churchill, S. W., "Natural Circulation in an Inclined Rectangular Channel Heated on One Side and Cooled on the Opposite Side," *International Journal of Heat and Mass Transfer*, Vol. 17, No. 10, 1974, pp. 1209–1217.